



ELSEVIER

Contents lists available at ScienceDirect

Microelectronic Engineering

journal homepage: www.elsevier.com/locate/mee

Research paper

Electronic transport parameters of indium zinc oxide thin films after Al₂O₃/HfO₂ top-dielectric formation annealingG.A. Umana-Membreno^{b,*}, Y. Song^{b,*}, N.D. Akhavan^a, J. Antoszewski^a, D.C. Paine^b, A. Zaslavsky^{b,c}, L. Faraone^a^a School of E. E. & C. Engineering, The University of Western Australia, Perth, WA 6009, Australia^b Dept. of Physics, Brown University, Providence, RI 02912, USA^c School of Engineering, Brown University, Providence, RI 02912, USA

ARTICLE INFO

Article history:

Received 5 March 2017

Received in revised form 8 May 2017

Accepted 13 May 2017

Available online 15 May 2017

Keywords:

IZO

TFT

Electron mobility

Hall-effect

Anisotropy

Reliability

ABSTRACT

Oxide-based dielectrics can be formed on indium zinc oxide (IZO) through oxidation of deposited metallic layer such as Al and Ti. The metal/IZO reactions necessary for dielectric oxidation tend to consume oxygen from the IZO channel and thus lead to the formation of oxygen-deficiency defects in the IZO layer. However, if the formation of such defects is significant at room temperature, it may adversely impact the long-term reliability of IZO devices. This work presents results of a study of electronic transport in IZO insulator/semiconductor structures measured immediately after the oxidizing anneal and 1 year thereafter. The sample measured 1 year after annealing exhibited a nearly one order of magnitude increase in electron concentration, indicating that donor-like defects are formed under ambient room temperature conditions. Furthermore, and in contrast to the isotropic nature of electron transport in the sample measured immediately after annealing, significant anisotropy in transport parameters was found in the sample measured 1 year after annealing.

© 2017 Published by Elsevier B.V.

1. Introduction

Transparent oxide amorphous semiconductors are attractive for electronic and optoelectronic devices on flexible, lightweight, and low-cost substrates, and are thus of particular interest for applications in large-area and high-resolution thin-film transistor (TFT) based displays [1–4]. For such applications, amorphous oxide semiconductors based on the In₂O₃–Ga₂O₃–ZnO alloy system offer large bandgaps, relatively high electron mobilities (>10 cm²/Vs), and can be deposited at low substrate temperatures [1–4]. While thin-films formed using either binary In₂O₃–ZnO (IZO) and ternary In₂O₃–Ga₂O₃–ZnO (IGZO) oxide alloys exhibit electron mobilities exceeding 10 cm²/Vs, Nomura et al. noted that, in IZO thin-films, electron concentrations below 10¹⁷ cm⁻³ are difficult to obtain, and tend to suffer carrier concentration controllability and stability problems due to the generation of excess carriers even under ambient conditions [2]. Amorphous In₂O₃ and ZnO thin-films, deposited at low substrate temperatures, have also been recently reported, with electron mobilities > 10 cm²/Vs [5–8]. However, the electron

concentration in such films was not detailed. It should be noted that, in general, the electron mobility in amorphous semiconductors of the In₂O₃–Ga₂O₃–ZnO alloy system depends on carrier concentration, this is due to the presence of potential barriers arising from structural randomness of the amorphous matrix, with the transport mechanism switching from thermally activated and percolation limited mobility for electron concentrations < 10¹⁹ cm⁻³, to degenerate-type and impurity scattering limited for higher electron concentrations [9].

Though IZO films have been reported with electron concentrations < 10¹⁵ cm⁻³ and mobilities > 1 cm²/Vs [10], Song et al. did not report details on the stability of such IZO layers. In contrast, it is known that the incorporation of Ga metal atoms in IGZO films tend to yield more stable and controllable carrier concentrations, since the formation of oxygen-deficiency defects is significantly suppressed [4]. While this suggests that IGZO is superior to IZO for TFT switching applications, IZO/IGZO bilayers are of interest to realise photo-TFT image sensor arrays [4].

In spite of these challenges, high performance top-gated IZO-based TFTs have been demonstrated using dielectric gate insulators formed by oxidation of a metallic layer (such as Al, Ti, etc.) via metal/IZO reaction during annealing at relatively low temperatures (200–300 °C) and/or via oxygen diffusion from the annealing

* Corresponding authors.

E-mail address: gilberto.umanamembreno@uwa.edu.au (G. Umana-Membreno).

ambient [11,12]. The metal/IZO reaction tends to consume oxygen from the IZO channel, thus leading to the formation oxygen-deficiency related defects in the IZO layer and to IZO channels that exhibit high n-type carrier density. However, if the rate of formation of oxygen-deficiency related defects is not negligible at room temperature, the long-term reliability of IZO devices thus realized would be adversely impacted. This work presents results of a study of electronic transport in IZO insulator/semiconductor structures measured immediately after annealing and after 1 year storage under ambient conditions.

2. Experiment and sample details

IZO-based insulator/semiconductor test-structures were fabricated on a Si substrate with a 500 nm thermally grown SiO_2 layer. The electrodes and IZO channel layer were patterned by conventional lithography and lift-off. The IZO channel was defined as a square-geometry Van der Pauw test structure (Fig. 1). As a first step, electrodes were formed by deposition of 10 nm Mo onto the SiO_2/Si substrate, which was followed by the formation of a Ag-nanoparticle rich layer as a low contact resistance ohmic layer [13]. The 40 nm-thick IZO thin-film was then deposited by DC magnetron sputtering, followed by the deposition of 2 nm Al by RF sputtering. On top of the previously defined ohmic contact regions additional layers of 20 nm Mo, 10 nm Cr and 70 nm Au were then deposited. A HfO_2 layer was subsequently deposited by atomic layer deposition, which was then removed from the contact regions. Further process details can be found in Refs. [11,13]. A micro-graph of a fabricated test structure and a schematic cross-sectional diagram are shown in Figs. 1 and 2.

The test structures, from adjacent areas in the same wafer region, were annealed for 8 h at 300 °C in air, to induce the formation of Al_2O_3 from the deposited Al metallic layer. Immediately prior to measurements, the samples were mounted on device holders, employing gold wire and Ag-loaded electrically conductive epoxy cured at 80 °C for 1 h. Magnetic-field dependent resistivity and Hall-effect measurements were performed employing a superconducting magnet system at magnetic field intensities up to $B = 10$ T, and sample temperatures ranging from 20 to 300 K.

3. Results and discussion

Initial room temperature measurements indicated significant differences in the electronic transport parameters of the two samples investigated. The sample measured immediately after annealing (Sample 1) exhibited relatively isotropic electrical characteristics, as can be seen from 4-terminal resistances presented in Fig. 3a,

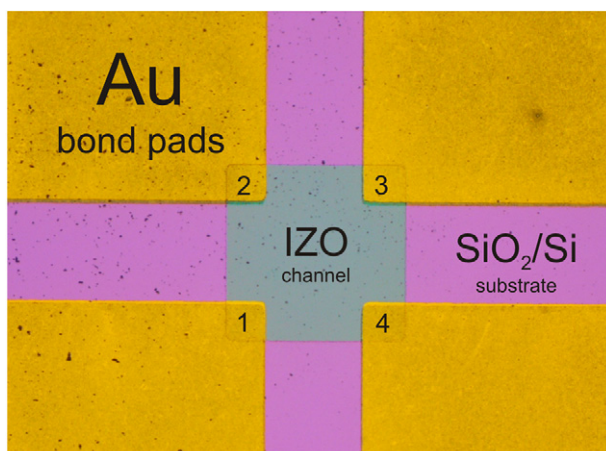


Fig. 1. Micro-graph of fabricated square-geometry Van der Pauw test-structure.

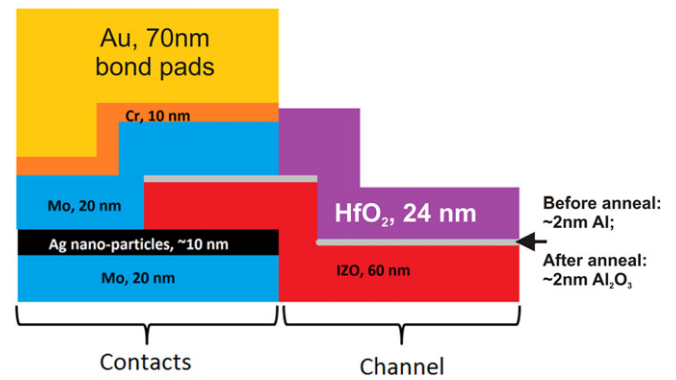


Fig. 2. Schematic cross-sectional diagram of the test structures employed in this study.

which were measured using the Van der Pauw test configuration. Conventional Hall-effect analysis, at a fixed magnetic field intensity of $B = 1$ T, indicated n-type conductivity with a high electron concentration of $1.59 \times 10^{19} \text{ cm}^{-3}$ and a mobility of $43.4 \text{ cm}^2/\text{Vs}$. In contrast, the sample measured one year after annealing (Sample 2) exhibited 4-terminal resistances which differed along the two parallel sets of contacts, suggesting significant anisotropy in transport

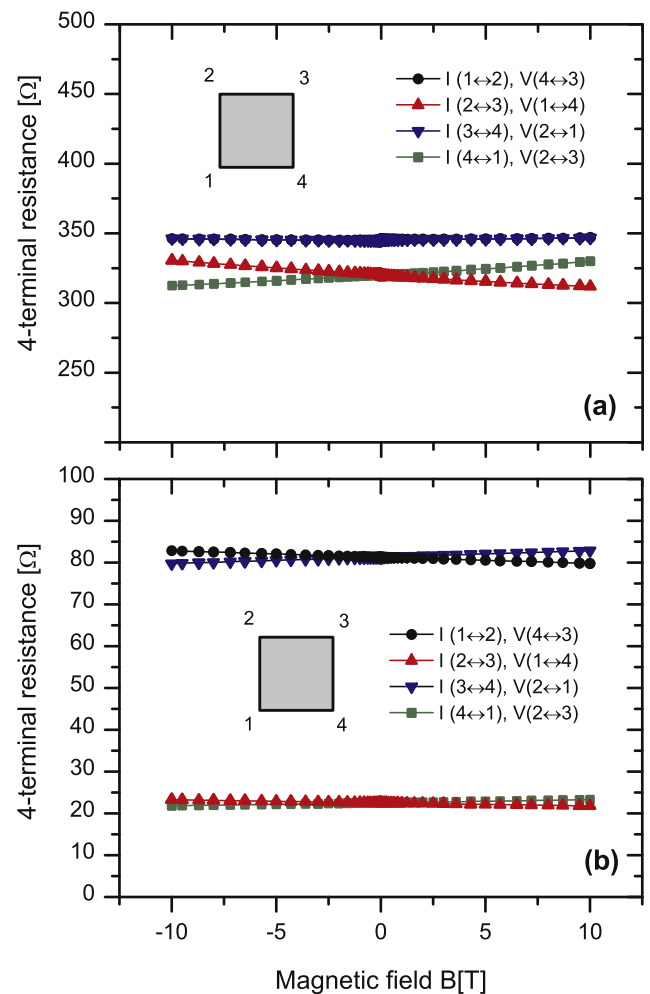


Fig. 3. Measured room-temperature magnetic-field-dependent 4-terminal resistances: (a) Sample measured immediately after annealing (Sample 1), and (b) Sample measured one year after annealing (Sample 2).

parameters, as shown in Fig. 3b. Neglecting this anisotropy, conventional Hall-effect analysis indicated n-type conductivity with a significantly higher electron concentration of $1.38 \times 10^{20} \text{ cm}^{-3}$ but with a lower mobility of $36.5 \text{ cm}^2/\text{Vs}$. If it is assumed that the electron concentration is isotropic, orthogonal mobilities associated with the resistivity components $\rho_{12,34}$ and $\rho_{23,41}$ can be extracted using the method of Bierwagen et al. by taking into account the square geometry of the sample [14]. Following this approach, two distinct orthogonal electron mobilities of $30.7 \text{ cm}^2/\text{Vs}$ and $43.3 \text{ cm}^2/\text{Vs}$ were extracted, with an isotropic electron concentration of $1.38 \times 10^{20} \text{ cm}^{-3}$.

Regarding the temperature dependence over the 20–300 K range, Sample 1 remained relatively isotropic, while the anisotropic characteristics of Sample 2 persisted, as shown by the extracted effective anisotropy ratio $A_{\text{eff}} = \rho_{12,34}/\rho_{23,41}$ characteristics plotted in Fig. 4. For both samples, the electron concentration was found to be approximately constant over the whole temperature range. Transport parameters extracted employing conventional Hall-effect analysis, at a magnetic field intensity of $B = 1 \text{ T}$, are summarized in Figs. 5 and 6, where, again, the orthogonal mobility components for Sample 2 were extracted using the method of Bierwagen et al. [14]. Interestingly, the temperature dependent electron mobility characteristics of Sample 1 and Sample 2 were found to differ significantly. The electron mobility in Sample 1 was found to decrease as the temperature was lowered, from $43.4 \text{ cm}^2/\text{Vs}$ at 300 K to $14.2 \text{ cm}^2/\text{Vs}$ at 20 K, indicating stronger electron scattering at lower temperatures. For $T \leq 80 \text{ K}$, the mobility followed a $T^{0.56}$ dependence. In contrast, Sample 2 exhibited electron mobilities that increased as the temperature decreased to 80 K, remaining nearly constant at lower temperatures. Though the temperature dependence of the extracted mobilities, for either the orthogonal component, appears consistent with lattice scattering, the mobility follows a $T^{-0.16}$ dependence which differs significantly from $T^{-1.5}$ expected for lattice-scattering limited mobility. This suggests that, although lattice scattering is acting to reduce the mobility at high temperatures, defect-related scattering is likely to play a dominant role in limiting electron mobility [15]. Screening, owing to the higher electron concentration in Sample 2, can thus explain the higher mobility values observed in this sample at $T < 80 \text{ K}$.

These observations are in agreement with the mobility and carrier concentration relationships in IZO films reported by Leenheer et al. and Martins et al. [15,16], and are also consistent with

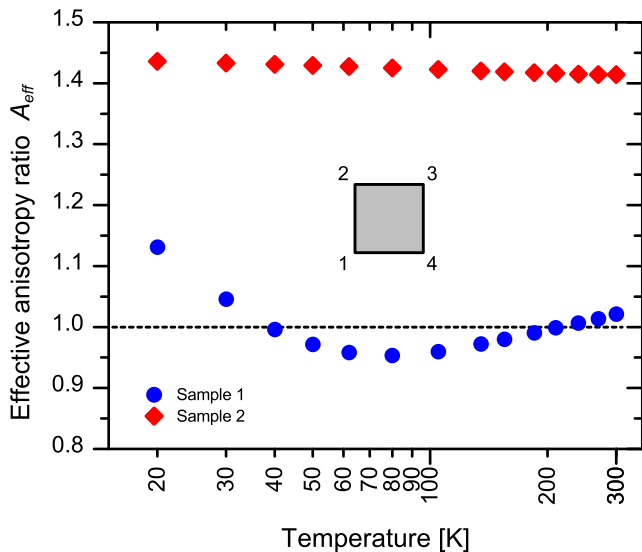


Fig. 4. Effective anisotropy ratio $A_{\text{eff}} = \rho_{12,34}/\rho_{23,41}$ at $B = 0 \text{ T}$, extracted employing the method in Ref. [14].

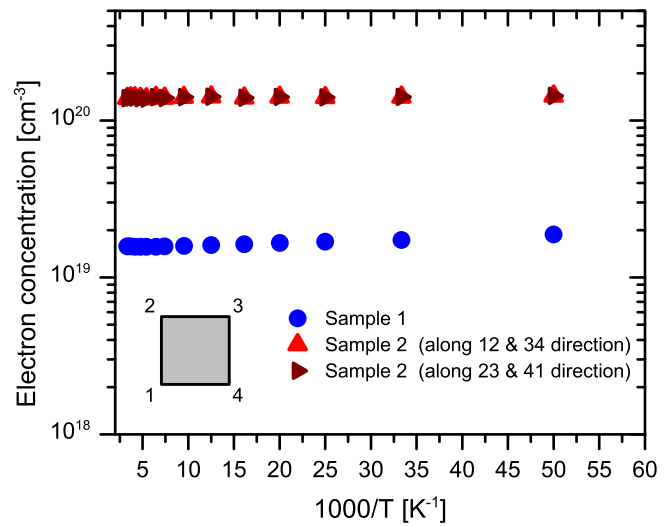


Fig. 5. Carrier concentration extracted from Hall effect measurements at $B = 1 \text{ T}$.

those reported for indium gallium zinc oxide (IGZO) thin-films [17]. However, the anisotropy in the conductivity of IZO films has not been previously reported. Since potential fluctuations in amorphous IZO films are expected to be random and thus isotropic, it is likely that the anisotropy observed in Sample 2 arises from regions exhibiting lower electron potential with long-range orientation defined by: (a) factors associated with sample fabrication and/or deposition conditions, rather than an intrinsic characteristic of IZO films; and/or (b) formation of donor-like defects, likely oxygen-deficiency related defects, with a preferential long-range orientation arrangement defined by deposition conditions and/or fabrication process. Since both samples are from adjacent regions in the wafer, the conduction anisotropy observed in Sample 2 (shown in Fig. 4) can be speculated to be an indicator of long-range orientation of defects during the post-annealing storage time. However, further studies will be necessary to clarify whether the observed anisotropy is solely due to IZO film deposition conditions.

High-resolution mobility spectrum analysis of magnetic field dependent Hall-effect and resistivity measurements at 300 K

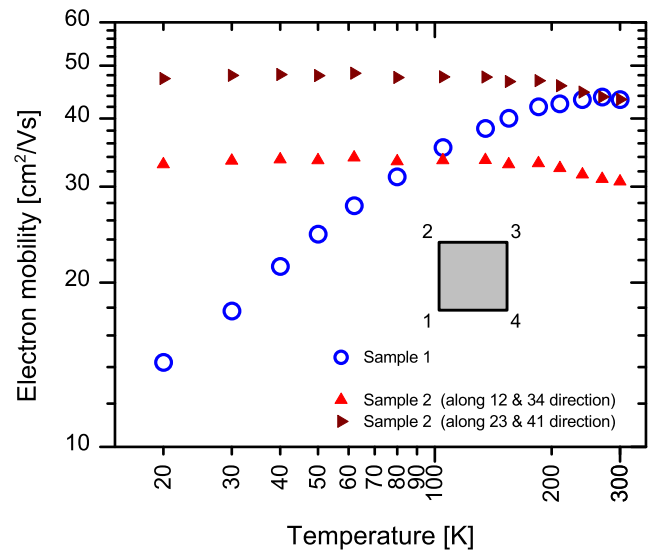


Fig. 6. Electron Hall mobility extracted from measurements at $B = 1 \text{ T}$. For Sample 2, the method of Bierwagen et al. has been employed to deconvolve orthogonal mobility components [14].

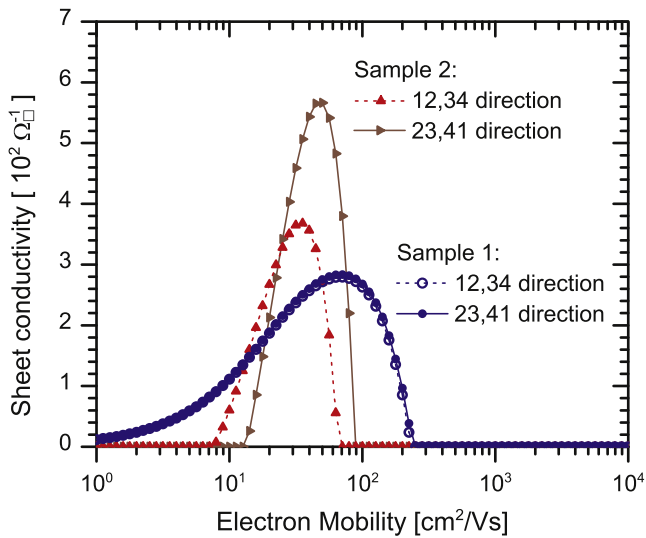


Fig. 7. Electron mobility spectra extracted from magnetic field dependent measurements.

revealed significant differences in the electron mobility distribution in the samples, as evidenced in Fig. 7. For Sample 2, the electron mobility spectra are noted to be relatively narrow, with Hall scattering factors r_H of 1.26 and 1.19 for the low and high mobility directions, respectively, whereas Sample 1 exhibited a very broad distribution with an extracted Hall scattering factor $r_H = 3.39$, suggesting that conventional Hall-effect analysis significantly underestimates the true electron concentration (since $n_D = r_H n_H$, with n_D and n_H denoting the drift and Hall electron concentrations, respectively) [18,19]. Mobility spectrum analysis of measurements performed at temperatures below 300 K was not possible due to negative magnetoresistance, which appears consistent with a model proposed by M.R. Boon [20]. Further details regarding negative magnetoresistance in the samples studied will be reported elsewhere.

4. Summary

Electronic transport characterization of IZO insulator/semiconductor structures has revealed significant change in electronic parameters in samples measured immediately after annealing and after 1 year storage under ambient conditions. The nearly one order of magnitude increase in electron concentration indicates an increase in donor density, likely associated with the formation of

oxygen-deficiency related defects at room temperature, as a consequence of continued oxidation of unreacted Al metallic species in the insulating Al_2O_3 layer. In contrast to the isotropic nature of electron transport in the sample measured immediately after annealing, significant anisotropy in transport parameters was found in the sample measured 1 year after annealing.

Acknowledgements

This work was supported by the Australian Research Council (DP140103667, LE110100200), and the Australian National Fabrication Facility. The Brown University-based co-authors (YS, AZ, and DCP) acknowledge the financial support of the National Science Foundation award DMR-1409590.

References

- [1] K. Nomura, H. Ohta, A. Takagi, T. Kamiya, M. Hirano, H. Hosono, *Nature* 432 (2004) 488.
- [2] K. Nomura, A. Takagi, T. Kamiya, H. Ohta, M. Hirano, H. Hosono, *Jpn. J. Appl. Phys.* 45 (2006) 4303.
- [3] T. Kamiya, K. Nomura, H. Hosono, *Origins of high mobility and low operation voltage of amorphous oxide TFTs: electronic structure, electron transport, defects and doping*, *J. Disp. Technol.* 5 (2009) 273.
- [4] A. Nathan, S. Lee, S. Jeon, J. Robertson, *J. Disp. Technol.* 10 (2014) 917.
- [5] Y.-H. Kim, J.-S. Heo, T.-H. Kim, S. Park, M.-H. Yoon, J. Kim, M.S. Oh, G.-R. Yi, Y.-Y. Noh, S.K. Park, *Nature* 489 (2012) 128.
- [6] D.B. Buchholz, Q. Ma, D. Alducin, A. Ponce, M. Jose-Yacamán, R. Khanal, J.E. Medvedeva, R.P.H. Chang, *Chem. Mater.* 26 (2014) 5401.
- [7] H.-H. Hsieh, C.-C. Wu, *Appl. Phys. Lett.* 91 (2007) 013502.
- [8] D.J. Rogers, V.E. Sandana, F.H. Teherani, R. McClintock, M. Razeghi, H.-J. Drouhin, *Proc. SPIE* 7940 (2011) 79401K.
- [9] H. Hosono, *Transparent Amorphous Oxide Semiconductors for Flexible Electronics*, Springer, Boston (USA), 2011, 459–487. (Ch. 13).
- [10] J.-I. Song, J.-S. Park, H. Kim, Y.-W. Heo, J.-H. Lee, J.-J. Kim, G.M. Kim, B.D. Choi, *Appl. Phys. Lett.* 90 (2007) 022106.
- [11] Y. Song, R. Xu, J. He, S. Siontas, A. Zaslavsky, D.C. Paine, *IEEE Electron Device Lett.* 35 (2014) 1251.
- [12] H. Ji, A.Y. Hwang, C.K. Lee, P.S. Yun, J.U. Bae, K.S. Park, J.K. Jeong, *IEEE Trans. Electron Devices* 62 (2015) 1195.
- [13] R. Xu, J. He, Y. Song, W. Li, A. Zaslavsky, D.C. Paine, *Appl. Phys. Lett.* 105 (2014) 093504.
- [14] O. Bierwagen, R. Pomraenke, S. Eilers, W.T. Masselink, *Phys. Rev. B* 70 (2004) 165307.
- [15] R. Martins, P. Barquinha, A. Pimentel, L. Pereira, E. Fortunato, *Phys. Status Solidi A* 202 (2005) R95.
- [16] A.J. Leenheer, J.D. Perkins, M.F.A.M. van Hest, J.J. Berry, R.P. O'Hayre, D.S. Ginley, *Phys. Rev. B* 77 (2008) 115215.
- [17] H. Yabuta, N. Kaji, M. Shimada, T. Aiba, K. Takada, H. Omura, T. Mukaide, I. Hirozawa, T. Koganezawa, H. Kumomi, *J. Phys. C* 518 (2014) 012001.
- [18] J. Antoszewski, G.A. Umana-Membreno, L. Faraone, *J. Electron. Mater.* 41 (2012) 2816.
- [19] G.A. Umana-Membreno, J. Antoszewski, L. Faraone, *Microelectron. Eng.* 109 (2013) 232.
- [20] M.R. Boon, *Phys. Rev. B* 7 (1973) 761.